Mapping Magnetic Susceptibility Anisotropies of White Matter in vivo in the Human Brain at 7 Tesla

Xu Li[1,2], Deepti S Vikram[1,2], Issel Anne L Lim[1,3], Craig K Jones[1,2], Jonathan A.D. Farrell[1,2], and Peter C.M. van Zijl[1,2]

[1]*F.M. Kirby research center for functional brain imaging, Kennedy Krieger Institute, Baltimore, MD, United States,* [2]*Radiology, Johns Hopkins University School of Medicine, Baltimore, MD, United States,* [3]*Biomedical Engineering, Johns Hopkins University School of Medicine, Baltimore, MD, United States*

Introduction: High resolution phase or frequency images acquired using gradient recalled echo (GRE) MRI at high field show tissue contrast related to magnetic susceptibility.[1] In addition, advances in the development of quantitative susceptibility mapping (QSM) make it possible to reproducibly image the intrinsic local susceptibility contrast.[2-5] However, recent studies also indicate that magnetic susceptibility in white matter is anisotropic and needs to be described by a second-order tensor.[6,7] Susceptibility tensor imaging (STI) of *ex vivo* mouse brain shows white matter structure quite similar to that obtained by diffusion tensor imaging (DTI),[7,8] suggesting the possibility of mapping susceptibility tensor elements assuming cylindrical symmetry of the white matter fibers.[9] Here, we propose a method to map the mean magnetic susceptibility (MMS) and magnetic susceptibility anisotropy (MSA) of brain tissue by combining GRE phase images collected at a small number of head orientations with the fiber direction information extracted from DTI.

Theory: Using STI theory, system equations were derived in Cartesian coordinates. In general for a second order susceptibility tensor $\bar{\bar{\chi}}$, the relative field change $\Delta B/B_0$ due to $\bar{\bar{\chi}}$ that can be measured by an MR scanner can be described as in Eq. (1)[7],

$$\delta B(\mathbf{k}) = \mathrm{FT}(\frac{\Delta B}{B_0}) = \frac{1}{3}\hat{\mathbf{H}}_0 \cdot \mathrm{FT}\{\bar{\bar{\chi}}\} \cdot \hat{\mathbf{H}}_0 - \hat{\mathbf{H}}_0 \cdot \mathbf{k}\frac{\mathbf{k} \cdot \mathrm{FT}\{\bar{\bar{\chi}}\} \cdot \hat{\mathbf{H}}_0}{k^2} \quad (1)$$

where FT denotes the Fourier transform and $\widehat{\mathbf{H_0}}$ is the unit vector in the direction of the of the main magnetic field. The field shift is measured in the lab frame, while the susceptibility tensor and field orientation in Eq. (1) are defined in the subject frame. In the subject frame, $\bar{\bar{\chi}}^{sub}$ can be further decomposed as $\bar{\bar{\chi}}^{sub} = \sum_{i=1}^{3} \chi_{ii}^{diag} \mathbf{v}_i \mathbf{v}_i^T$, where χ_{ii}^{diag} is the susceptibility eigenvalue in the diagonal frame and $\mathbf{v}_i$ is the susceptibility eigenvector. By assuming the susceptibility tensor $\bar{\bar{\chi}}^{sub}$ has the same principle axis as the diffusion tensor $\bar{\bar{\mathbf{D}}}^{sub}$, we know $\mathbf{v}_i$ from DTI, and by assuming a cylindrical symmetry for $\bar{\bar{\chi}}^{diag}$ as shown in Fig. 1a, i.e. letting $\chi_{11}^{diag} = \chi_{\parallel}$ and $\chi_{22}^{diag} = \chi_{33}^{diag} = \chi_{\perp}$, we can rewrite Eq. (1) as in Eq. (2), where the MMS and MSA are defined as $\chi_{avg} = \frac{1}{3}(2\chi_{\perp} + \chi_{\parallel})$ and $\chi_{ani} = \chi_{\parallel} - \chi_{\perp}$, respectively, and $\bar{\bar{\mathbf{T}}} = \mathbf{I} - 3\mathbf{v}_1\mathbf{v}_1^{\mathrm{T}}$, where $\mathbf{I}$ is identity matrix and $\mathbf{v}_1$ is the principle eigenvector of $\bar{\bar{\chi}}^{sub}$ and $\bar{\bar{\mathbf{D}}}^{sub}$. With n (n>=2) phase/frequency measurements at different head orientations[9], we can then solve Eq. (2) for the MMS and MSA.

$$\delta B(\mathbf{k}) = \frac{1}{3}\hat{\mathbf{H}}_0 \cdot \mathrm{FT}\{\chi_{avg} - \frac{1}{3}\chi_{ani}\bar{\bar{\mathbf{T}}}\} \cdot \hat{\mathbf{H}}_0 - \hat{\mathbf{H}}_0 \cdot \mathbf{k}\frac{\mathbf{k} \cdot \mathrm{FT}\{\chi_{avg} - \frac{1}{3}\chi_{ani}\bar{\bar{\mathbf{T}}}\} \cdot \hat{\mathbf{H}}_0}{k^2} \quad (2)$$

Methods: An iterative LSQR based solver was developed to solve Eq. (2). For the simulation study, four head orientations were used (normal position, rotation about the y(AP) axis by +/-30°, rotation about the x(RL) axis by 30°). Figure 1b shows the diagram of the head phantom. Reconstruction performance was tested under noise free conditions then for phase data with an SNR of 30 and DTI eigenvectors that had Gaussian noise with a standard deviation of 10 degrees. For the *in vivo* human study, phase images were acquired using 3D multi-echo GRE MRI on 3 healthy male subjects at 7T (1mm isotropic resolution, TR/TE/ΔTE=45/2/2 ms, 9-16 echoes) with four different head orientations. All data were coregistered in the subject frame based on the AC-PC axis and mid-saggital plane, and the angles between this frame and the field (lab frame) was calculated from scanner angulation parameters. DTI data were collected on the same subjects at 3T (2.2mm isotropic resolution, 32 gradient orientations) and coregistered to the GRE magnitude images, then analyzed in the subject frame. The GRE multi-echo phase images were unwrapped using a Laplacian based method[4] and linearly fitted and converted to field maps. The background gradient field was removed by a dipole fitting method.[10]

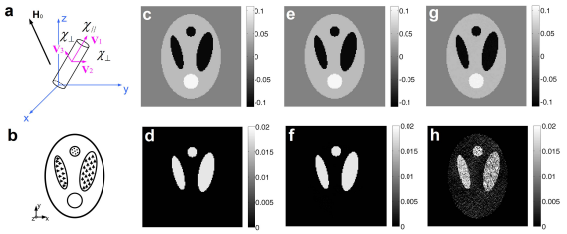

Fig. 1 (a) Diagram of the susceptibility tensor. (b) Diagram of the head phantom. (c, d) target MMS and MSA maps in ppm units. (e,f) reconstructed MMS and MSA maps for noise free condition. (g, h) MMS and MSA maps for SNR of 30 in the phase maps.

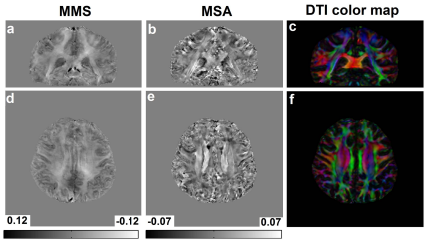

Fig. 2 (a and d) MMS maps. Note that negative MMS is displayed bright (b and e) MSA maps. Positive MSA is bright (c and f) DTI color maps. Unit is ppm.

ROIs	MMS (ppm)		MSA (ppm)	
	Mean	SD	Mean	SD
IC	-0.0305	0.0008	-0.0089	0.0012
EC	-0.0244	0.0021	-0.0092	0.0055
TR	-0.0351	0.0035	0.0061	0.0031
CR	-0.0238	0.0018	0.0062	0.0020
CG	-0.0181	0.0009	0.0009	0.0021
CC	-0.0249	0.0021	0.0176	0.0009

Table 1 MMS and MSA values (n = 3) in selected white matter fibers (calculated from mean values of three subjects).

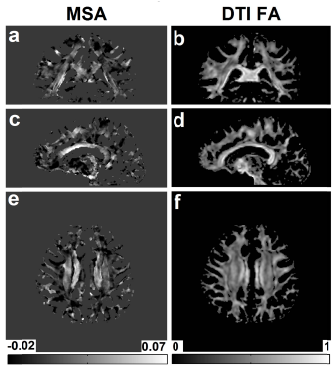

Fig. 3 MSA map versus FA map

Results and Discussion: Figure 1 shows the target MMS and MSA maps of the head phantom (c, d) and the reconstructed MMS and MSA maps under noise free conditions (e, f). The MMS and MSA maps obtained under noisy conditions are shown in Figures 1g and 1h, with relative reconstruction errors of 2% and 65% for MMS and MSA, respectively. Figure 2 shows examples of MMS and MSA maps of a single subject in comparison to the corresponding DTI color map. The MMS maps show good contrast between white and grey matter. In most central white matter fibers, the MSA exhibits slightly positive values, except fibers around the globus pallidus, such as the internal capsule. In addition, the MSA map is relatively noisy around tissue interfaces which may be caused by registration error. Figure 3 shows a comparison between the MSA maps and the corresponding DTI FA maps of a single subject. Here a white matter mask with FA>0.25 is applied on both the MSA and the FA maps. The MMS and MSA values for selected white matter fibers are summarized in Table 1. Abbreviations in Table 1 are as follows: IC: internal capsule; EC: external capsule; TR: thalamic radiations (including optic radiations); CR: corona radiata; CG: cingulum; CC: corpus callosum.

Conclusions: A method to produce MMS and MSA images using phase data collected at four head orientations with respect to the main magnetic field was demonstrated in simulation and subsequently applied to whole brain phase data acquired *in vivo* on three healthy subjects at 7T. The results show that MMS maps show good contrast between gray and white matter, while MSA maps reveal most of the major central white matter fiber bundles.

References: [1] Duyn JH, et al. PNAS, 2007, 104(28):11796-11801. [2] Wharton S, et al. NeuroImage, 2010, 53(2):515-525. [3] Liu T, et al. MRM, 2011, 66(3):777-783. [4] Li W, et al. NeuroImage, 2011, 55(4):1645-1656. [5] Schweser F, et al. NeuroImage, 2011, 54(4):2789-2807. [6] Lee J, et al. PNAS, 2010, 107(11):5130-5135. [7] Liu C, MRM, 2010, 63(6):1471-1477. [8] Mori S, et al. AnnNeurol, 1999, 45(2):265-269. [9] Wharton S, et al. ISMRM 2011, #4515. [10] de Rochefort L, et al. MRM, 2010, 63(1):194-206. **Funding**: NIH/NCRR-P41 RR015241